

## Multi-Scale Ballistic Impact Simulation of Dry Woven Fabric with Elastic Crimped Fibers

Ala Tabiei<sup>a</sup> and Gaurav Nilakantan

*Dept. of Aerospace Engineering and Engineering Mechanics,  
University of Cincinnati, OH 45221, USA*

<sup>a</sup>*Corresponding Author, Email: ala.tabiei@uc.edu*

### ABSTRACT:

*A material model has been developed to realistically simulate the behavior of loose woven fabrics with elastic crimped fibers subject to varying loading conditions such as in-plane and transverse loading. It is based upon a multi-scale micromechanical approach that includes the architecture of the fabric and the phenomenon of fiber reorientation, with fiber simplified as one dimensional elastic members with a single failure criterion. The material model is implemented as a user-defined subroutine in the explicit, non-linear dynamic finite element code LSDYNA. Results of fabric test simulations run in LSDYNA using this material model agree well with experimental results, demonstrating the material model's capability to accurately simulate ballistic impact of woven fabrics.*

### KEYWORDS:

*Computational micro-mechanical material model; flexible woven fabric; ballistic impact simulations; nonlinear explicit finite element analysis; LSDYNA; protective structures*

### CITATION:

A. Tabiei and G. Nilakantan. 2011. Multi-scale ballistic impact simulation of dry woven fabric with elastic crimped fibers, *Int. J. Vehicle Structures & Systems*, 3(2), 74-79. doi:10.4273/ijvss.3.2.01

## 1. Introduction

With the advent of high modulus and high strength fibers since the 1960s, various ballistic applications have utilized the effective projectile penetration resistance and impact energy dissipation offered by fabrics composed of these fibers. These include protective clothing for military and law enforcement personnel, protective layering in turbine fragment containment, armor plating of vehicles, commercial aircraft and helicopter secondary composite parts, particularly facings of honeycomb sandwich constructions, boat hulls, electrical and electronic parts, and coated fabrics. Considerable research has been conducted into modeling the complex behavior of these fabrics and capturing the various fabric phenomena such as yarn reorientation and pullout during in-plane loading and transverse ballistic experiments. With the parallel advent of supercomputing and commercial finite element codes, emphasis is now on numerically simulating physical phenomena through various techniques of which the finite element method is popular.

This research presents a micromechanical based technique to treat the fabric behavior with yarns idealized as elastic members with a single mode failure criterion. A representative multi-scale volume cell (RVC) approach is used to represent the overall fabric structure and equilibrium of the central nodes at yarn crossover points is used to calculate yarn stresses and strains. Yarn crimp and reorientation are automatically handled by the material model. The material model is implemented as a user defined subroutine in the explicit

finite element code LSDYNA. Fabric tensile test simulations are run in both the axial and bias directions and compared to experimental results. Next, ballistic impact simulations are run and compared to experimental findings.

There are many approaches that can be used to model fabric behavior under loading conditions and arrive at the constitutive equations, with each method having its own advantages. They include analytical methods, empirical methods, numerical methods, micromechanical methods, multi-scale constitutive methods, variational methods, and experimental methods. A comprehensive review paper of the state of the art in analysis, simulation, and experimental characterization of woven fabric can be found in reference [1]. Reference [1] lists more than 175 journal papers on this topic and therefore literature review in the current paper is omitted.

## 2. Representative Multi-Scale Volume Cell

The representative volume technique, vastly used in the micro-mechanical models, is utilized hereafter. A current deformed state of the fabric is considered. The Representative Volume Cell (RVC) of the loosely woven fabric material model is extracted from the deformed pattern of the material. The RVC consists of an undulated fill yarn crossed over an undulated warp yarn. The original RVC model used in this paper is based on the model developed by the principle author and presented in reference [2].

In explicit finite element codes as LS-DYNA, the material model have to determine the stress response of the material to the strain increment obtained at each time step of the explicit time integration. Assuming that the RVC coordinate system is the shell element local coordinate system, the stress response of the woven fabric RVC to the strain increment passed to the model in the RVC coordinate system has to be developed by the micro-mechanical approach.

### 3. Elasticity Model

The governing equation of elasticity for the one element elastic model can be derived from equilibrium as

$$\sigma = K_a \varepsilon \quad (1)$$

Then Eqn. (1) can be written in incremental form for the time step  $n+1$  as follows:

$$\sigma^{(n)} + \Delta\sigma^{(n)} = K_a (\varepsilon^{(n)} + \Delta\varepsilon^{(n)}) \quad (2)$$

We can determine the stress increment from the last equation,

$$\Delta\sigma^{(n)} = K_a (\varepsilon^{(n)} + \Delta\varepsilon^{(n)}) - \sigma^{(n)} \quad (3)$$

Where  $K_a$  is the spring stiffness and is equal to  $E_1$ , the static Young's modulus of elasticity. The only failure mode available is when the fiber strain reaches the failure strain or

$$\varepsilon = \sigma / K_a > \varepsilon_{max} \quad (4)$$

The input parameters for the Elasticity model are Hookean spring coefficient  $K_a$  and static ultimate strain  $\varepsilon_{max}$  (see Fig. 1).



Fig. 1: One Element Elasticity Model

We now consider the equilibrium position of the central nodes on the center of the undulation as seen in Fig. 2. We consider the equilibrium of the central nodes (the crossover point) of the yarns at time step  $n+1$  because the incremental elasticity equations of the yarns are written for this instant. Again we assume that this state is linear interpolation of the states at time step  $n$  and time step  $n+1$ . The equilibrium state is given in Fig. 2 for the fill yarn (upper scheme) and for the warp yarn (lower scheme). The span between the yarns and the length of the bars can be calculated for each time step of interest as follows:

$$s_f^{(n+1)} = \Lambda_f^{(n+1)} s, \quad s_w^{(n+1)} = \Lambda_w^{(n+1)} s \quad (5)$$

Substituting yarn strain increments of Eqn. (11) in Eqn. (10) and plugging Eqn. 6 in, we can get the final equation after some small simplifications:

$$\begin{aligned} & (h_f^{(n)} + \delta^{(n)}) \sqrt{(s_w^{(n+1)}/2)^2 + (h_w^{(n)} - \delta^{(n)})^2} * \left[ 2K_a \varepsilon_f^{(n)} - \sigma_f^{(n)} + \frac{K_a}{L} \left( \sqrt{(s_f^{(n+1)}/2)^2 + (h_f^{(n)} + \delta^{(n)})^2} - L_f^{(n)} \right) \right] \\ & + (\delta^{(n)} - h_w^{(n)}) \sqrt{(s_f^{(n+1)}/2)^2 + (h_f^{(n)} + \delta^{(n)})^2} * \left[ 2K_a \varepsilon_w^{(n)} - \sigma_w^{(n)} + \frac{K_a}{L} \left( \sqrt{(s_w^{(n+1)}/2)^2 + (h_w^{(n)} - \delta^{(n)})^2} - L_w^{(n)} \right) \right] = 0 \end{aligned} \quad (13)$$

$$\begin{aligned} L_f^{(n+1)} &= \sqrt{(s_f^{(n+1)}/2)^2 + (h_f^{(n)} + \delta^{(n)})^2}, \\ L_w^{(n+1)} &= \sqrt{(s_w^{(n+1)}/2)^2 + (h_w^{(n)} + \delta^{(n)})^2} \end{aligned} \quad (6)$$

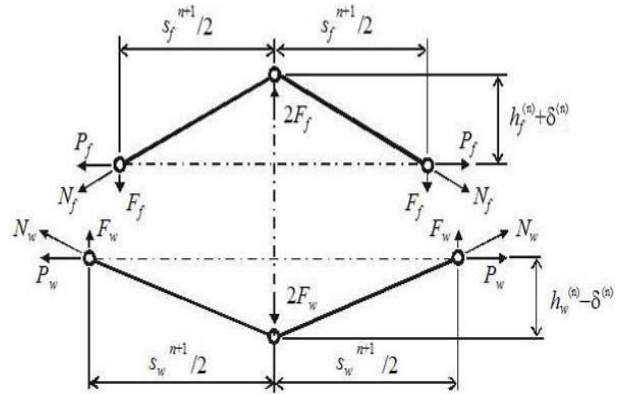


Fig. 2: Equilibrium position of the central nodes at the center of the undulation between the fill and warp

The vertical components of the yarn forces can be determined as follows:

$$F_f = \frac{h_f^{(n)} + \delta^{(n)}}{L_f^{(n+1)}} N_f = \frac{h_f^{(n)} + \delta^{(n)}}{L_f^{(n+1)}} (\sigma_f^{(n)} + \Delta\sigma_f^{(n)}) S \quad (7)$$

$$F_w = \frac{h_w^{(n)} + \delta^{(n)}}{L_w^{(n+1)}} N_w = \frac{h_w^{(n)} + \delta^{(n)}}{L_w^{(n+1)}} (\sigma_w^{(n)} + \Delta\sigma_w^{(n)}) S \quad (8)$$

where  $S$  is the cross-sectional area of the yarns. The equilibrium of the mechanism is reached when

$$2F_f = 2F_w \quad (9)$$

Developing Eqn. (9) by substituting in Eqns. (6) and (3) we get:

$$\begin{aligned} & \frac{h_f^{(n)} + \delta^{(n)}}{L_f^{(n+1)}} [2K_a \varepsilon_f^{(n)} + K_a \Delta\varepsilon_f^{(n)} - \sigma_f^{(n)}] S \\ & = \frac{h_w^{(n)} + \delta^{(n)}}{L_w^{(n+1)}} [2K_a \varepsilon_w^{(n)} + K_a \Delta\varepsilon_w^{(n)} - \sigma_w^{(n)}] S \end{aligned} \quad (10)$$

The strain increments of the yarns are determined by the expressions:

$$\Delta\varepsilon_f^{(n)} = (L_f^{(n+1)} - L_f^{(n)}) / L, \quad \Delta\varepsilon_w^{(n)} = (L_w^{(n+1)} - L_w^{(n)}) / L \quad (11)$$

Where  $L$  is the initial length of the bars calculated by the formula:

$$L = \sqrt{(s/2)^2 + (t/4)^2} \quad (12)$$

Eqn. (13) can be solved numerically for  $\hat{\delta}^{(n)}$  by means of Newton-Raphson method. The vertical position change of the central nodes is constrained in order to avoid the snap-through behavior of the mechanism,  $-t/4 \leq \delta^{(n)} \leq t/4$ . In this way, the buckling of the yarns in compression is represented by the structural buckling of the membrane shell element model. The vertical positions of the central nodes, initially set to  $h_f^{(0)} = h_w^{(0)} = t/4$ , are finally updated:

$$h_f^{(n+1)} = h_f^{(n)} + \hat{\delta}^{(n)}, \quad h_w^{(n+1)} = h_w^{(n)} + \hat{\delta}^{(n)} \quad (14)$$

#### 4. Stress Calculation

The actual lengths of the bars at time step  $n+1$  are calculated using Eqn. (6). Then the strain increments in the yarns are calculated by means of Eqn. (11) and the strain in the yarns can be updated:

$$\varepsilon_f^{(n+1)} = \varepsilon_f^{(n)} + \Delta\varepsilon_f^{(n)}, \quad \varepsilon_w^{(n+1)} = \varepsilon_w^{(n)} + \Delta\varepsilon_w^{(n)} \quad (15)$$

Applying Eqn. (3) for the fill and the warp yarns, we obtain the stress increments in the yarns,  $\Delta\sigma_f$  and  $\Delta\sigma_w$ . The stress in the yarns is updated for the next time step:

$$\sigma_f^{(n+1)} = \sigma_f^{(n)} + \Delta\sigma_f^{(n)}, \quad \sigma_w^{(n+1)} = \sigma_w^{(n)} + \Delta\sigma_w^{(n)} \quad (16)$$

We can imagine that the RVC is smeared to a parallelepiped in order to transform the stress acting on the yarn cross-section to the stress acting on the element wall. The thickness of the membrane shell element used should be equal to the effective thickness,  $t_e$ , that can be found by dividing the areal density of the fabric by its mass density. The in-plane stress components acting on the RVC walls in the material direction of the yarns are calculated as follows:

$$\sigma_{f11}^{(n+1)} = \frac{2\sigma_f^{(n+1)}S}{st_e}, \quad \sigma_{w11}^{(n+1)} = \frac{2\sigma_w^{(n+1)}S}{st_e} \quad (17)$$

$$\sigma_{f22}^{(n+1)} = \sigma_{f22}^{(n)} + \alpha E_2 \Delta\varepsilon_{f22}^{(n)}, \quad (18)$$

$$\sigma_{w22}^{(n+1)} = \sigma_{w22}^{(n)} + \alpha E_2 \Delta\varepsilon_{w22}^{(n)}$$

$$\sigma_{f12}^{(n+1)} = \sigma_{f12}^{(n)} + \alpha G_{12} \Delta\varepsilon_{f12}^{(n)}, \quad (19)$$

$$\sigma_{w12}^{(n+1)} = \sigma_{w12}^{(n)} + \alpha G_{12} \Delta\varepsilon_{w12}^{(n)}$$

where  $E_2$  is the transverse Young's modulus of the yarns,  $G_{12}$  is the longitudinal shear modulus, and  $\alpha$  is the lateral contact factor. The lateral contact factor is zero when the trellis mechanism is open and unity if the mechanism is locked with full lateral contact between the yarns. The yarn 2-D stress tensors,  $\sigma_f$  and  $\sigma_w$ , built up from the components calculated by Eqns. (17) – (19) are transformed to the RVC coordinate system:

$$\bar{\sigma}_f = \mathbf{T}_f^T \cdot \sigma_f \cdot \mathbf{T}_f, \quad (20)$$

$$\bar{\sigma}_w = \mathbf{T}_w^T \cdot \sigma_w \cdot \mathbf{T}_w$$

Then the final stress response of the model can be compiled from the yarn and the frictional stresses in RVC coordinate system as follows:

$$\sigma_x = \frac{\bar{\sigma}_{fxx} + \bar{\sigma}_{wxx}}{2} + \hat{\sigma}_x, \quad \sigma_y = \frac{\bar{\sigma}_{fyy} + \bar{\sigma}_{wyy}}{2} + \hat{\sigma}_y, \quad (21)$$

$$\sigma_{xy} = \frac{\bar{\sigma}_{fxy} + \bar{\sigma}_{wxy}}{2}$$

Where  $\hat{\sigma}_x, \hat{\sigma}_y$  are the frictional stresses between the yarns as defined in reference [2].

The membrane shell element formulation does not have resistance against the warping of quad finite elements and this could cause some instability in 3-D finite element models. This could be avoided by introducing transverse shear stiffness and calculating the transverse shear stresses in the shell element formulation.

#### 5. Numerical Results and Discussion

Because the behavior of the yarn has been represented by a one-element linear spring system, there is no strain rate or viscoelastic effect present. This implies that regardless of the strain rate in the fabric material during loading or deformation, the stress-strain response will remain the same. However in reality, all high strength and high modulus fabrics exhibit varying degrees of viscoelasticity. But representing a yarn as a simple elastic member is a common approach which greatly simplifies the formulation as well makes the numerical model less computationally expensive with good accuracy. Moreover, it acts as a simple platform on which various modifications and additions can be made to the model such as adding yarn pullout effect, remote yarn failure, and other complex phenomena, after which the yarn behavior can then be easily switched back to being viscoelastic.

##### 5.1. Tensile Test Simulations

To test the developed micromechanical material model under in-plane loading conditions, axial and bias tensile test simulations are conducted on a Kevlar S706 strip using LSDYNA. Axial tests refer to the case when the strip is pulled along the direction of the primary yarn. Bias tests refer to the case when the strip is pulled along a 45 degree angle to the primary yarn. The numerical setup is displayed in Fig. 3. The fabric strip is modeled with shell elements that utilize the developed material model. Two sets of quasi static tensile tests have been numerically simulated and compared to experimental findings from King et al. [4]. The first set involves pulling the fabric strip along the yarn direction and the second set involves pulling along the bias direction.

For the axial tests, a fabric strip with dimensions 25.4 mm x 355.6 mm was used. During the experiments, one end of the fabric was rigidly clamped while the other end was pulled at a rate of 0.01 s<sup>-1</sup>. For the bias tests, the fabric measured 35 mm x 95 mm and was pulled at a rate of 1 mm/s. While numerically simulating the quasi static test, the total simulation time used was 800 ms. Simulations run with a 400 ms run time displayed identical results. This implied that the speeding up of the quasi static tensile tests to a certain point did not affect the results and allowed the simulations to run in a reasonable time period.

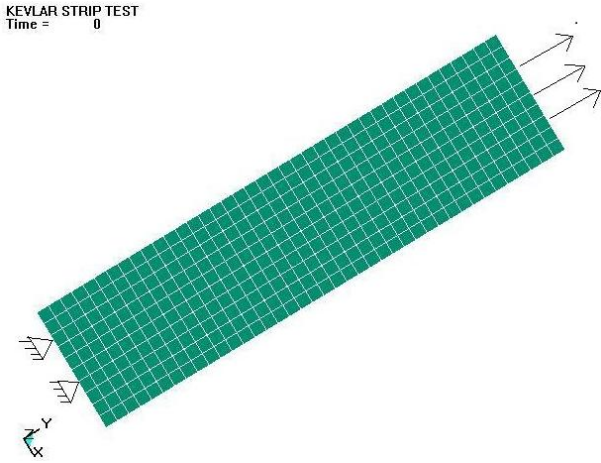


Fig. 3: Numerical setup of fabric axial strip test

The material properties of the fabric used in the experiments are as listed in Table 1. Some of the parameters input into the developed user defined material model are as listed in Table 2. Because fabrics have very low out of plane stiffness, using extremely small values of shear moduli can cause numerical instabilities and are therefore scaled higher in the material model. This does not alter the behavior of the fabrics in any way. Usually, choosing the in-plane shear moduli to be at least 0.1 times the longitudinal modulus of elasticity will prevent the rotation of the material integration points which may otherwise lead to hourglassing. In LSDYNA, this can also be prevented by using hourglass controls.

Table 1: Fabric material properties used in the experiments

Property Description	Value
Fabric	Kevlar S706
Yarn type	Kevlar KM2 600 denier
Number of warp/fill yarns	34 / inch
Fabric thickness	0.23 mm
Areal density	180 g/m <sup>2</sup>
Elongation at break	3.6%
Longitudinal Young's modulus	81 GPa
Tenacity	3400 MPa
Ultimate Tensile Strength	2040 MPa

Table 2: Input parameters to the user defined material model for in-plane tensile and ballistic testing

Property Description	Tensile test	Ballistic test
Longitudinal Young's modulus	81 GPa	96 GPa
Transverse Young's modulus	1.5 GPa	7.4 GPa
Shear modulus (G12)	1 GPa	2.5 GPa
Shear modulus (G23)	2 GPa	2 GPa
Yarn failure strain ( $\epsilon_{fail}$ )	3.6%	3.5%
Fabric real thickness	0.23 mm	
Fabric effective thickness	0.125 mm	
Locking angle	34.7 deg	
Initial braid angle	45 deg	
Transition Angle	3 deg	
Coefficient of friction ( $\mu$ )	1.7	
Primary spring stiffness (Ka)	5000 N/mm	
Yarn width (w)	0.262 mm	
Yarn cross sectional area (S)	4.63E-02 mm <sup>2</sup>	
Yarn span (s)	0.747 mm	

The results of the fabric strip tensile test simulations run in LSDYNA have been compared to the experimental findings of King et al. [4] and displayed in Figs. 4 and 5. The results agree very well with each other. Fabric tensile tests enable the testing of whether a user defined fabric material model can capture complex fabric phenomena such as fiber reorientation and locking. These phenomena cannot be adequately observed during the ballistic impact testing which is in the transverse direction.

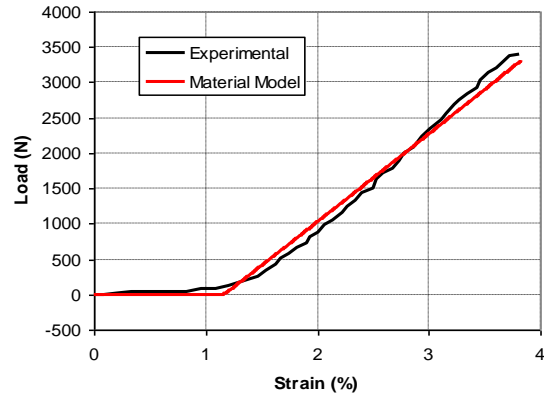


Fig. 4: Load-Strain plot of axial test

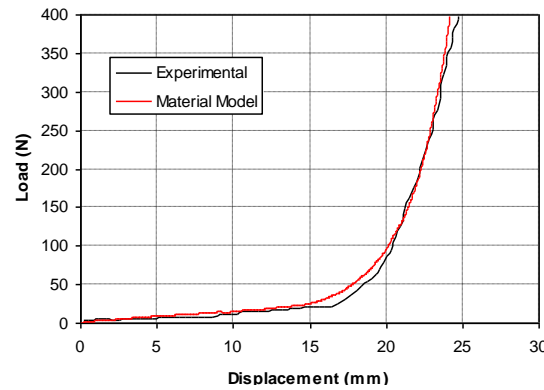


Fig. 5: Load-Displacement plot of bias test

From the axial strip tests in Fig. 4, we observe that the initial load-displacement curve is almost flat till a strain of 1.2%. Physically this means the yarns begin to straighten out (crimp reduction) as they are pulled along either the warp or weft direction until the undulation angle reaches a minimum and then the yarns begin to bear the full load. After this, the load-displacement behavior is almost linear. The developed material model implicitly updates the undulation angle at each time step through the span and yarn thickness variables (see Eqns. (5) and (14)). This is derived from the pin joint mechanism seen in Fig. 6 where,

$$\tan \beta = (\text{thickness} / 4) / (\text{span} / 2) \quad (22)$$

From the geometry and parameters used in the inputfile of the material model, the span is 0.747 mm and the fabric thickness is 0.23 mm. Thus, we obtain the initial undulation angle as 8.75°. To confirm this, we look at the load-displacement plot of the axial test. Since the load bearing capacity is almost zero until a strain of 1.2%, this means that the fabric initially stretches up to a distance of 4.331 mm before bearing any load.

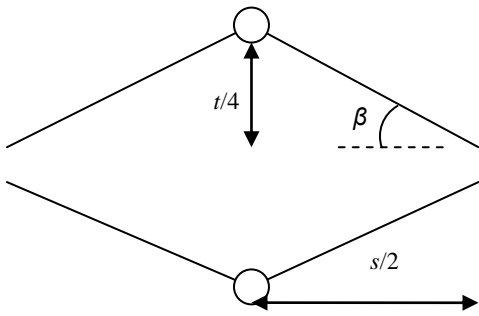


Fig. 6: Calculation of undulation angle  $\beta$

We can also calculate the undulation angle using this data. The projected length of the fabric on the x-y plane and therefore the projected length of the undulating warp yarns is 355.7 mm. If we were to stretch out these warp yarns until they were straight, their length would be  $(355.7 + 4.331)$  mm which yields 359.931 mm. The undulation angle can now be calculated as:

$$\cos \beta = 355.6 / 359.931 \quad (23)$$

This yields an initial undulation angle of  $8.897^\circ$ . Thus we obtained similar undulation angles both theoretically and numerically. From the bias test results in Fig. 5, we see that the load bearing capacity of the yarns increases very gradually up to a displacement of around 17 mm after which the yarns begin to sustain rapidly increasing loads. This is attributed to the initial reorientation of the yarns until yarn locking occurs. A degree of non-linearity can be observed in the load-displacement plot during the yarn locking phase as the discount coefficient increases from 0 to 1. After the yarns reach their locking angle, they are able to sustain the maximum load. During reorientation, the rotational friction of the yarns at the cross over points is responsible for the initial minimal load carrying capacity of the yarns.

### 6. Ballistic Impact Simulations

The ballistic impact of a RCC projectile onto a woven fabric target was simulated in LSDYNA. The target was composed of 8 layers of plain weave Kevlar 129 with each layer measuring 203 x 203 mm. Opposite edges of the target were rigidly clamped while the other two edges were left free. The projectile had a mass of 2.8 g and a diameter of 5.38 mm, with an initial velocity of 341 m/s. Some of the parameter inputted to the material model are listed in Table 2. The fabric was modeled using shell elements.

Experimental results from Starratt et al. [3] are used to compare results obtained from the material model. The spring constant used in the material model can be determined either experimentally or approximately from Eqn. (24) which is derived from Hooke's law:

$$F = EA \frac{\Delta d}{d} = k \Delta d \quad (24)$$

$$k = EA / d = (96E + 03)(4.63E - 02) / (1.00)$$

where  $E$  is the longitudinal modulus of elasticity of the yarn,  $A$  is the yarn cross sectional area, and  $d$  is the yarn length taken as unity. Eqn. (24) yields a spring constant of 4444.8 N/mm. The elastic stiffness of the spring used

in the one-element model that represented yarn behavior was chosen as 5000 N/mm as it gave the best results.

The deformation of the fabric at various time instants can be observed in Figs. 7 and 8. A pyramidal deformation shape can be observed which is also obtained experimentally. A measure of creasing can be observed in the middle of the fabric, parallel to the clamped ends. The stress wave and transverse deformation rapidly propagate to the clamped ends and get reflected back as can be seen in Fig. 9. The transverse deformation however does not propagate fully to the ends which are left free which is also observed experimentally for targets gripped only on two opposite edges. There is no perforation as the fabric target is able to completely retard the projectile's motion. Due to limitations in the measurement system of the experimental testing of [3], the entire history of the projectile velocity and fabric deflection could not be obtained and was limited to a maximum window of 25 mm which corresponded to the width of the laser sheet used in the ELVS system. Further, differences in clamping pressure used in the experiments led to differing results for the same impact event. Some amount of fabric slippage at the boundaries was also present which induced errors into the experimental results.

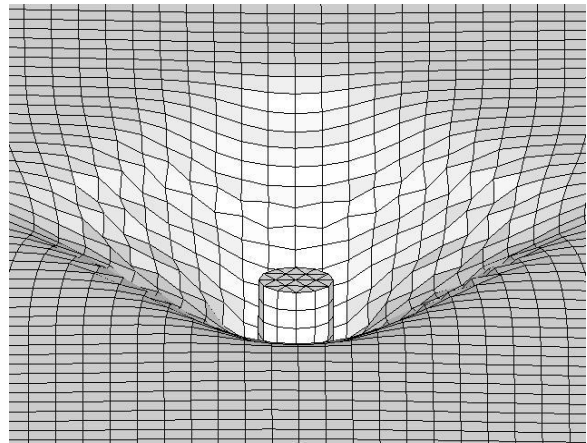


Fig. 7: Close up of the fabric deformation

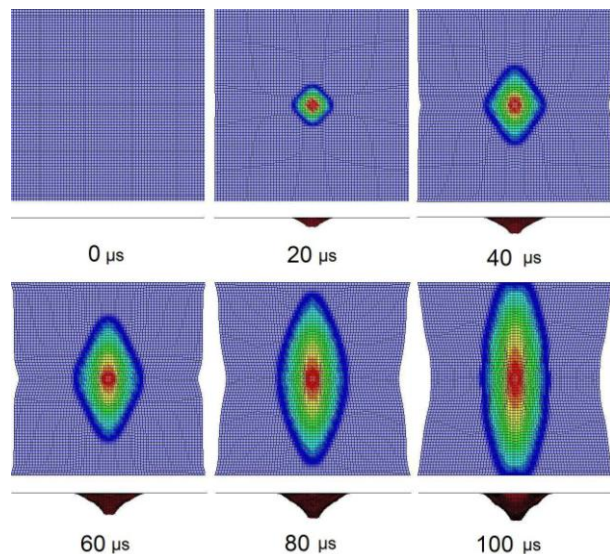


Fig. 8: States of fabric deformation at various time instants

Figs. 9 and 10 display the projectile's displacement and velocity history respectively. There is very good agreement between the results.

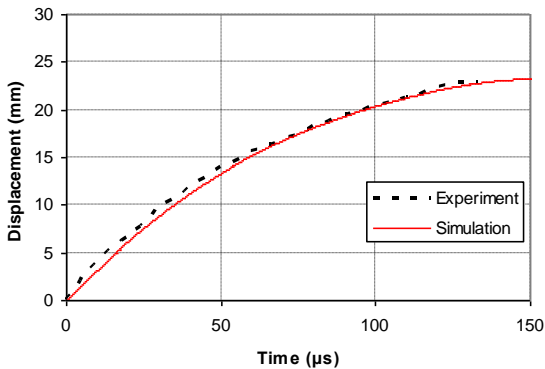


Fig. 9: Projectile displacement

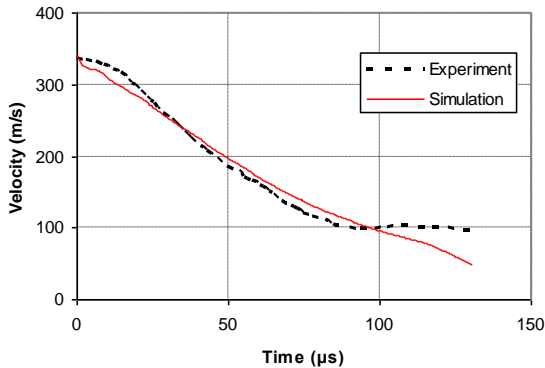


Fig. 10: Projectile velocity

Figs. 11 and 12 display the contact force between the projectile and target, and energy absorbed by the fabric respectively. The response of the elastic yarns in the fabric display a stiffer initial reaction than the actual viscoelastic yarns in the experiment as seen in Fig. 11, leading to a sharp increase in contact force and correspondingly an increased initial energy absorption by the fabric as predicted by the material model. This difference in results may also partly be by virtue of the contact algorithm used in LSDYNA that uses a penalty formulation to calculate contact forces.

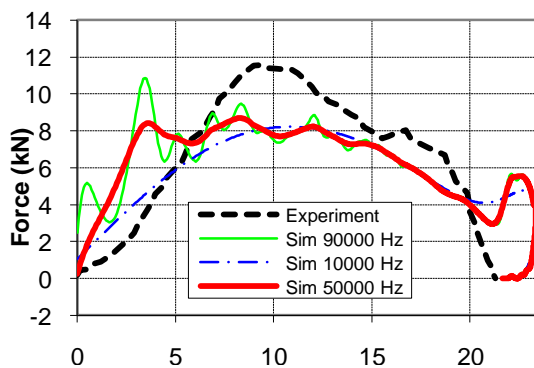


Fig. 11: Contact force between projectile and fabric filtered at different frequencies

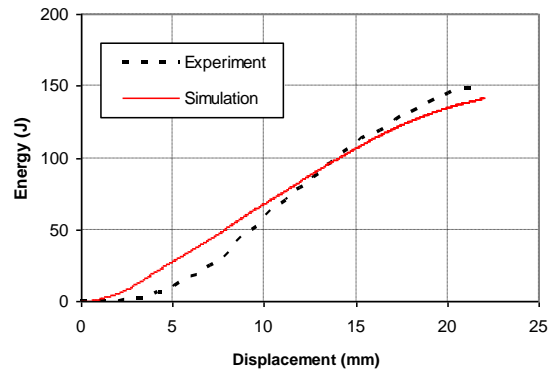


Fig. 12: Energy absorbed by the fabric

## 7. Conclusions

The presented material model can accurately represent fabric behavior during in-plane tensile loading in both the axial and bias directions. Yarn undulations are implicitly included in the representative volume cell approach used. Fabric phenomena such as yarn reorientation and locking have been captured by the material model. Rotational frictional effects have been included as the yarns rotate at the cross over points. A simple strain to failure criteria has been included. The material model also accurately represents fabric behavior during transverse ballistic impact. A pyramidal deformation shape was obtained which is also observed during experiments. The good agreement between the material model predictions and experimental results demonstrates the material model's capability to be accurately used for simulating ballistic impact of woven fabrics in commercial FE codes.

## ACKNOWLEDGEMENT:

The authors gratefully acknowledge the computing support provided by the Ohio Supercomputing Center.

## REFERENCES:

- [1] A. Tabiei and G. Nilakantan. 2008. Ballistic impact of dry woven fabric composites: A review, *Applied Mechanics Review*, 61(1), 10801-10813. doi:10.1115/1.2821711
- [2] A. Tabiei and I. Ivanov. 2002. Computational micro-mechanical model of flexible woven fabric for finite element impact simulation, *Int. J. Numerical Methods in Engineering*, 53, 1259-1276. doi:10.1002/nme.321
- [3] D. Starratt, G. Pageau, and R. Vaziri. 1999. An instrumented experimental study of the ballistic impact response of Kevlar fabric, *Proc. 18<sup>th</sup> Int. Symp. Ballistics*, San Antonio, Texas, USA.
- [4] M.J. King, P. Jearanaisilawong, and S. Socrate. 2005. A continuum constitutive model for the mechanical behavior of woven fabric, *Int. J. Solids & Structures*, 42, 3867-3896. doi:10.1016/j.ijsolstr.2004.10.030